# Data Repository Item 2010270

# Wide-angle traveltime analyses, refraction velocity models, and additional single-channel seismic record sections

Seismic velocities are critical for determining the depth of the bottom-simulating reflector (BSR), which can be compared to measurements of the depth of the glide plane of the frontal ridge slide. In this Item, supporting information is presented to demonstrate how seismic velocities were obtained beneath the frontal ridge (section DR.1), and to illustrate the nature of the resulting seismic velocity model which includes a well-constrained BSR at a depth of 255 (±15) mbsf (section DR.2). Additional vertical-incidence seismic sections show the nature of the BSR distribution along the ridge and perpendicular to it, and also further illustrate the prominent seafloor scarps and associated faults along the top of the ridge (section DR.3).

## DR.1. Determination of velocities from wide-angle reflections and refractions

In 2005, eight ocean bottom seismometers (OBSs) were deployed in a grid pattern at a nominal separation of 650 m on the frontal ridge (Figure DR1). OBS D was positioned at Site U1326 of the Integrated Ocean Drilling program (IODP). The seismic source, fired every 10 or 11 s, was a GI-gun configured with a 105 cu. in. generator and a 105 cu. in. injector. Single channel seismic (SCS) lines were recorded simultaneously with the OBS recording. Eight seismic lines were collected.

An OBS may drift a hundred meters or more from its deployment position before it reaches its rest position on the seafloor, so it is necessary to determine the final OBS position from the recorded data. Since accurate shot positions were known from the ship's navigation, the direct arrival for each of the many shots recorded on each OBS was used in a traveltime inversion procedure to determine the OBS position, given an accurate water velocity profile. The positioning error, represented by the traveltime residual from all shots, was ±10 m for OBS A, D, G, and H on the crest of the ridge, and approximately ±30 m for other OBSs on the steeper slopes of the ridge. The accuracy in water depth at each OBS was estimated as ±5 m.

The velocity structure on the frontal ridge was determined using the traveltime inversion routine of Zelt and Smith (1992). A 2D velocity model was determined along three lines – line 2 through four OBSs, line 3 through 3 OBSs, and line 8 through 2 OBSs (Figure DR1). Line 8 is perpendicular to the margin, while lines 2 and 3 are parallel to the margin through the long axis of the ridge. For each profile, the model was constrained simultaneously by traveltimes from wide-angle reflections and refractions recorded on the OBSs, and from vertical-incidence reflections recorded on the coincident single-channel seismic lines. Velocity model construction was an interactive process that combined both inversion and forward modeling. A sample dataset for OBS D and the final ray trace through the velocity model for line 2 is shown in Figure DR2. The events that were observed on all OBSs and were subsequently modeled include (a) an early event (P2) from shallow depths (<100 m) with an apparent velocity of ~2.0 km/s, (b) the wide-angle reflection from the bottom-simulating reflector (BSR, or P3) or base of hydrate, and (c) a strong refraction (P4) with a high velocity of ~2.4 km/s. Vertical-incidence traveltimes for the BSR from the coincident SCS line (essentially identical to line 13 in Fig. 2) were also modeled simultaneously.

Information about the reliability of the traveltime inversion is given by the root-mean-square (rms) traveltime residual and the $\chi^2$ normalized misfit parameter. Pick uncertainties were typically ~20 ms for the OBS and vertical-incidence arrivals. The modeling continued until $\chi^2$ had a value near 1, which indicates that the observed data have been fit to within their assigned uncertainties. In order to estimate uncertainty in the solution, a sensitivity analysis was performed by perturbing the depth parameters, following the procedure of Katzman et al. (1994). Typical depth errors for the BSR and shallower horizons were ±15 m, with corresponding velocity errors of ±50-100 m/s.

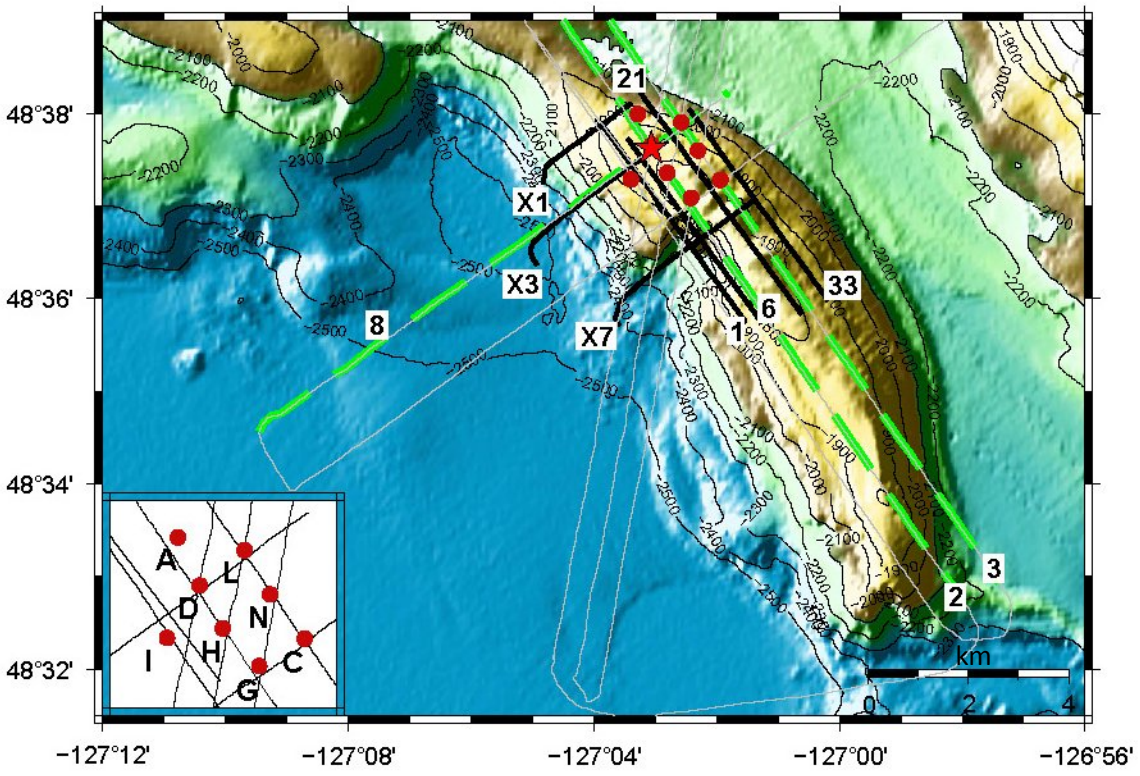


**Figure DR1.** The seafloor positions of a grid of 8 ocean bottom seismometers (OBSs) with a nominal separation of 650 m are shown by the red circles, and a detailed view with OBS names is given in the insert. 2D seismic velocity models beneath the frontal ridge were determined by traveltime inversion of coincident wide-angle and single-channel seismic data, from shots along three profiles (green dashed lines); additional wide-angle profiles are indicated by the thin grey lines, but these were not used in the present interpretation. The velocity model from profile 2 is shown in Figure DR3. Solid black lines are locations of single-channel seismic profiles (Figures DR6 and DR7) that indicate structure beneath the ridge. Site U1326 is indicated by the red star.

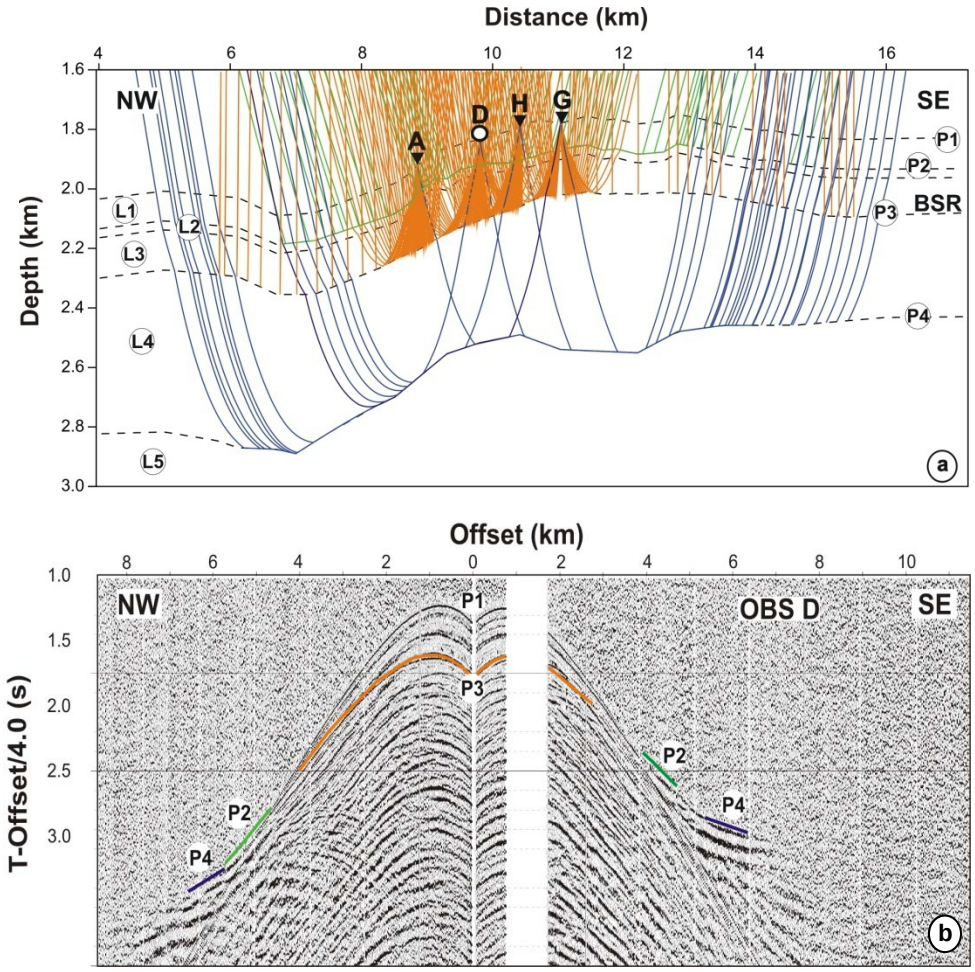


**Figure DR2.** (a) Reflected and refracted rays along line 2 parallel to the margin, through OBS A, D, H and G. IODP Site U1326 is located very close to OBS D. Green rays correspond to refractions P2 from just beneath the Layer1/Layer2 interface; blue rays correspond to refractions P4 from just beneath the layer 4/Layer 5 interface. Orange rays are reflections from the base of layer 3 (BSR); vertical-incidence reflections from SCS line 2 are represented by the vertical orange rays. Traveltimes for all refractions and wide-angle reflections were inverted simultaneously to determine the velocity model. The overall root-mean-square traveltime residual for this model is 18 ms, which is close to the picking error. (b) Vertical component of OBS D data along line 2 and picked arrivals (solid lines, with the same color scheme as for the rays in (a)).

## DR.2. Seismic velocity structure and gas hydrate concentrations on the frontal ridge

The seismic velocity structure beneath the frontal ridge, including the depth to the BSR, is well-constrained by simultaneous modeling of consistent events observed on multiple OBSs and on single-channel seismic profiles. The velocity model beneath line 2 is shown in Figure DR3. The velocity model is in agreement with logging results from Site U1326 of the Integrated Ocean Drilling Program (Figure DR4), located at OBS D of the seafloor OBS grid. The main features of the velocity model include the following:

1) A high-velocity layer at depths of 80-110 mbsf (layer L2) was found with velocities of 1.95 (±0.05) km/s, in contrast with average velocities of ~1.52 km/s between the seafloor and the top of layer L2. At Site U1326, wireline logging showed even higher P-wave velocities Figure DR4), varying from 1.75 to >2.8 km/s, as well as a very high resistivity section from 72 to 107 mbsf; this interval likely represents thin layers with high and low concentrations of gas hydrates, with gas hydrate saturations of 30-60% (Riedel et al., 2006).

2) The BSR depth beneath line 2 is about 240-260 mbsf. Beneath SCS line 3 (see Figure DR1 for location), BSR depths increase to near 280 mbsf. Water depths increase from about 1800-2100 m beneath line 2 to 1850-2100 m beneath line 3. For a change in water depth from 1800 m to 2100 m, the increase in pressure is expected to produce an increase in BSR depth of about 10 m. However, the sub-seafloor temperature profile may also change from the top of the ridge to its base. Temperatures may decrease due to more lateral heat loss on the slope than on the top of the ridge (Ganguly et al., 2000), while temperatures may increase due to increased fluid flow along the main frontal thrust fault.

For layer L3 located just above the BSR, with a thickness of about 150 m, the average velocity is well-constrained at 1.90 (±0.05) km/s. The velocity gradient is not well determined from the wide-angle data, since no observed refractions turn within this layer; hence, the gradient was simply set to be the same as the average gradient from the P-wave sonic logs at Site U1326. Hydrate saturations were estimated using an effective porosity-reduction method, in conjunction with an empirical velocity-porosity relation (Yuan et al., 1996). For layer L3 the average hydrate saturation is ~25% of the pore space, and varies from about 18% at the top to 32% at the base, depending on the assumed velocity gradient.

3) For layer L4 beneath the BSR, the refraction data constrain only the average velocity as ~2.0 km/s with an average thickness of about 420 (±50) m. The resolution of the method is insufficient to determine whether or not there is a thin gas layer just beneath the BSR.

Based on the observation of a BSR on single-channel seismic data (Figure DR5), hydrate is distributed over a wide region beneath the ridge. The BSR is observed mainly over the crest and part of the seaward flank region, plus a region northwest of the base of the ridge.

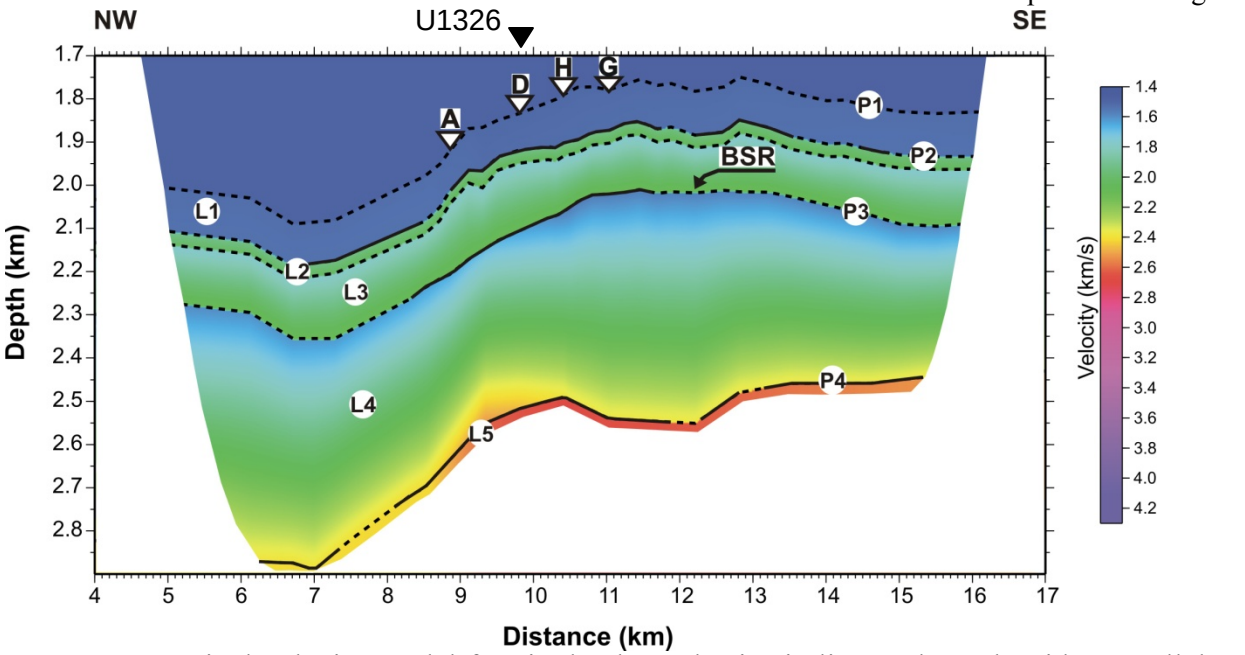


**Figure DR3.** Final velocity model for single-channel seismic line 2 along the ridge parallel to the margin. The model is constrained by wide-angle reflections and refractions recorded on OBSs A, D, H and G (indicated by inverted triangles) and by vertical-incidence BSR reflections from line 2. Solid lines indicate the ray coverage for the different interfaces. The BSR is well-constrained at an average depth of 255 (±15) mbsf beneath this profile. Model is identified by layers L1 to L4, and interfaces P1 to P4 (for details, see caption for Figure DR2).

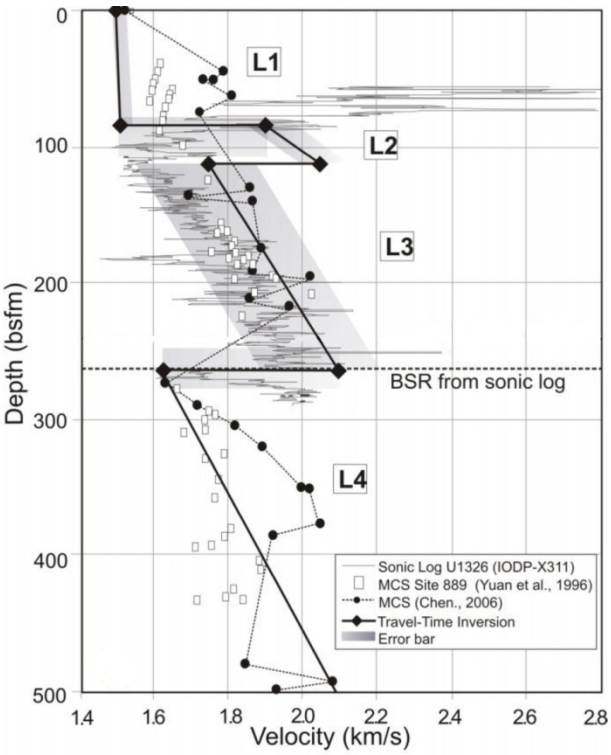


**Figure DR4.** Refraction velocities (black line) at intersection of line 2 and 8, located at the drillhole Site U1326. Sonic log for U1326 is the grey line. Filled circles and open squares are multichannel seismic velocities of Yuan et al. (1996) and Chen (2006), respectively. Error bar determined by inversion sensitivity analyses is indicated by shaded region.

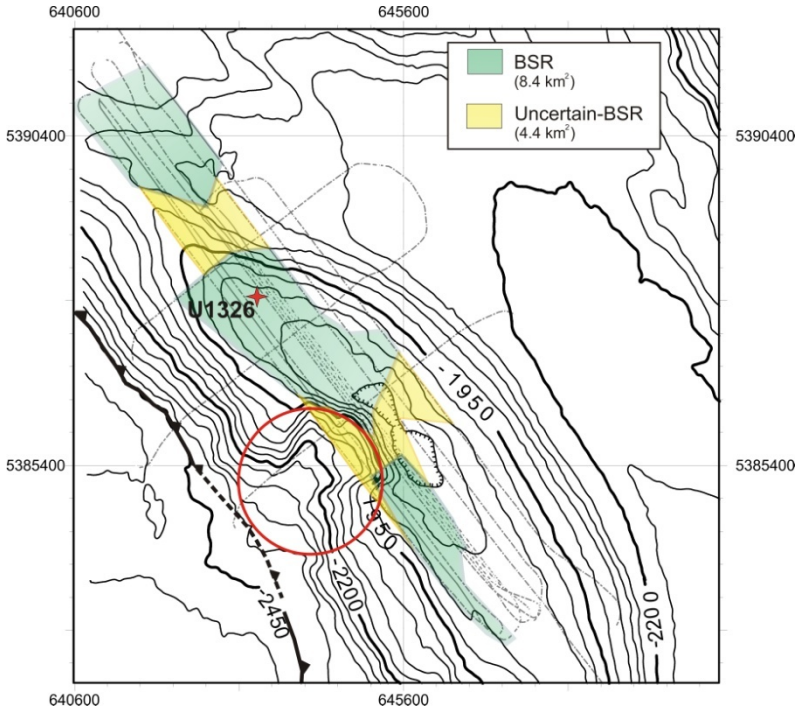


**Figure DR5.** Map of distribution of BSR based on single-channel seismic lines from cruise PGC0408. Green polygons correspond to areas with BSR clearly identified; yellow polygons correspond to areas of uncertain BSR. The red circle identifies the slide on the steep slope of the frontal ridge near IODP Site 1326, just landward of the deformation front (dashed line).

## DR.3. Additional single-channel seismic lines across the frontal ridge

Seismic line X1 (Fig. DR6a) is perpendicular to the margin and crosses the northern flank of the frontal ridge. A BSR is seen clearly beneath the entire line, extending from the shallowest water depths of 1900 m to the west end of the line at water depths of 2200 m.

Seismic line X7 (Fig. DR6b) passes through the slump, perpendicular to the headwall and the deformation front. Steep slopes are very difficult to image using only single-channel seismic techniques, and even the seafloor reflection is poorly imaged. There is no indication that the BSR has been re-established beneath the headwall or glide plane, but if present it would also be difficult to image. The strongest reflectivity beneath the seafloor is due to sub-horizontal stratigraphy that intersects the seafloor at an oblique angle, particularly beneath the headwall and upper portion of the glide plane. Hence, the headwall and glide plane cut through the existing stratigraphy, and did not develop along a continuous stratigraphic horizon.

A series of seismic lines parallel to the margin (Figure DR7) show the continuity of seafloor scarps and related faults. As seen on the location map (Figure DR1), lines 1 and 6 cross the upper portion of the slide; line 6 crosses the headwall, while line 1 may cross the top of the glide plane. On these two lines, the BSR is present beneath most of the ridge, but it terminates sharply at the edges of the slide region. That is, the BSR has not had time to re-establish since the slide occurred.

## References

Katzmann, R., Holbrook, W., and Paull, C., 1994, Combined vertical-incidence and wide-angle seismic study of a gas hydrate zone, Blake Ridge: Journal of Geophysical Research, v. 99, p. 17975-17996.

Ganguly, N., Spence, G.D., Chapman, N.R., Hyndman, R.D., 2000, Heat flow variations from bottom simulating reflectors on the Cascadia margin: Marine Geology, v. 164, p 53-68.

Riedel, M., Collett, T., Malone, M., and the Expedition 311 Scientists, 2006, *Proceedings of the Integrated Ocean Drilling Program, Volume 311*: Washington, DC (Integrated Ocean Drilling Program Management International, Inc.); doi:10.2204/iodp.proc.311.2006.

Yuan, T., Hyndman, R., Spence, G., and Desmons, B. 1996. Velocity structure of a bottom-simulating reflector and deep sea gas hydrate concentrations on the Cascadia continental slope: Journal of Geophysical Research, v. 101, p. 13655-13671.

Zelt, C., and Smith, R., 1992. Seismic traveltime inversion for 2-D crustal velocity structure: Geophysical Journal International, v. 108, p. 16-34.

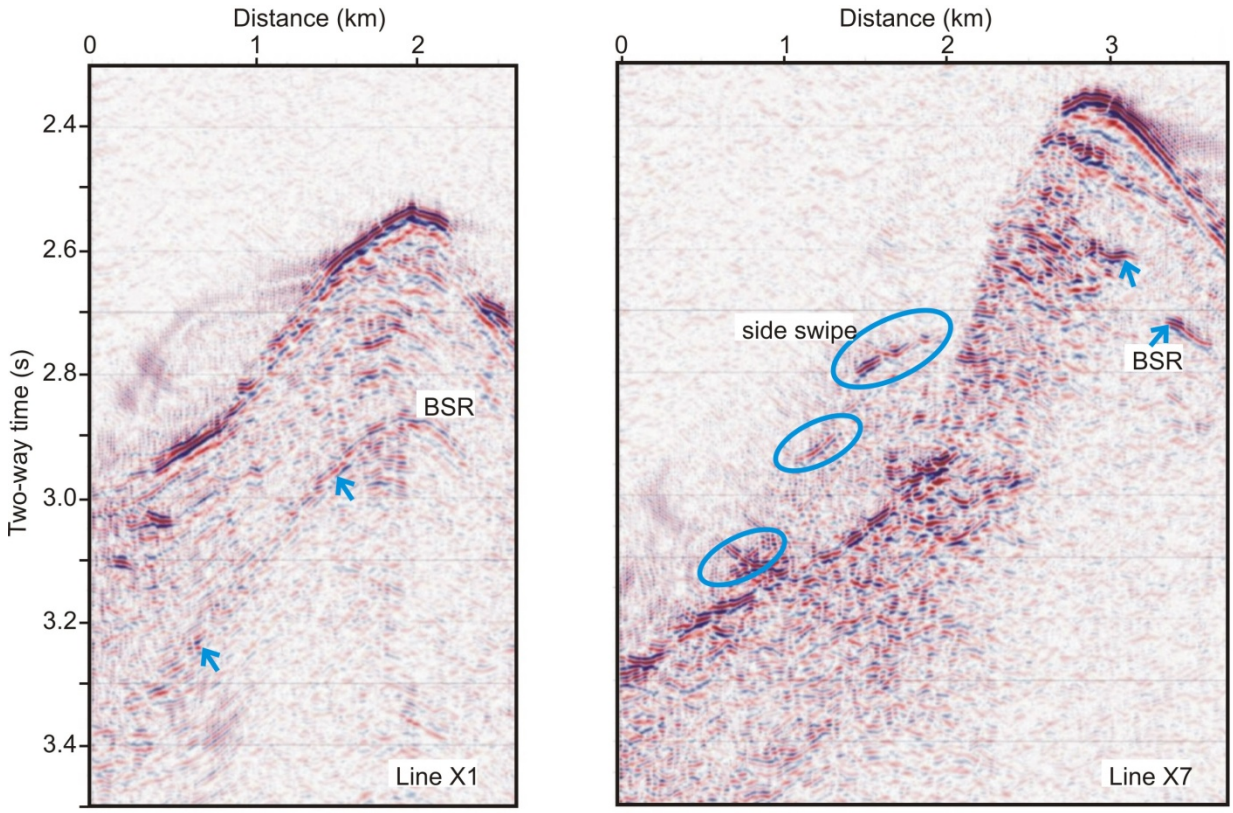


**Figure DR6.** Migrated single channel lines perpendicular to the margin; for locations, see Fig. DR1. Line X1 is located 1 km NW of IODP Site U1326; a BSR is clearly seen beneath this line. Line X7 crosses the slide headwall, 2 km SE of U1326; a BSR is seen only at the top of the ridge and on its landward slope, and not beneath the headwall or glide plane of the slide. Note that the stratigraphy on the seaward slope beneath line X7 is mostly at a high angle to the seafloor, and so the headwall and glide plane did not develop along a continuous stratigraphic layer. Side-swipe, or a series of reflections from the sidewall of the slump, is identified on line X7.

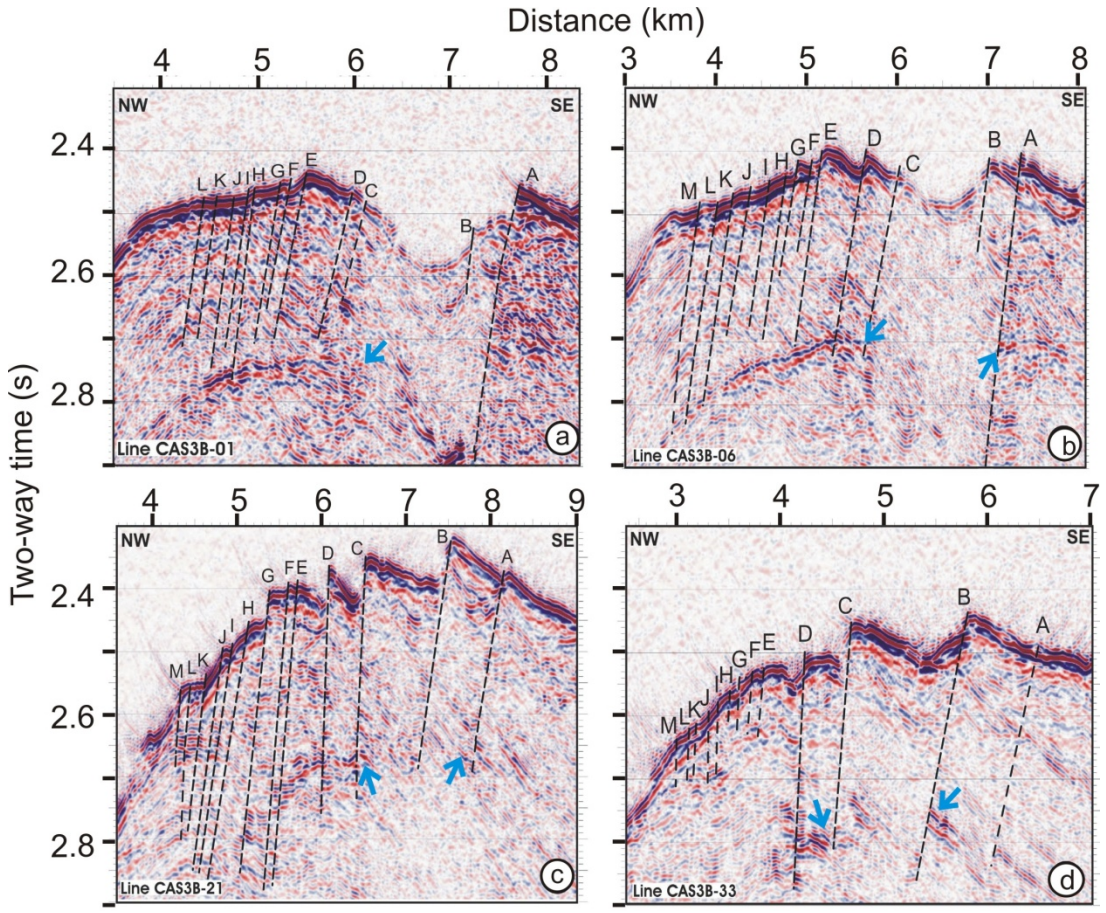


**Figure DR7.** Migrated single-channel seismic lines parallel to the margin: (a) line 1 (b) line 6 (c) line 21 (d) line 33. Locations of the seismic lines are shown in Figure DR1. Seafloor scarps, indicated by letters at the seafloor, are consistent from line to line – as mapped in Figure 1 of the main article. Lines 1 and 6 cross the top of the slide, which extends mostly between scarps A and C on these lines. Note that the BSR terminates near the edges of the slide (blue arrows), which on most lines is a region of little reflectivity. That is, the BSR has not had time to re-establish since the slide occurred.